Pergamon

Int. J. Heat Mass Transfer. Vol. 37, Suppl. 1, pp. 447–456, 1994

0017–9310/94 $6.00 + 0.00

0017–9310(93)E0061–K

Unsteady turbulent forced convection in a parallel-plate channel with timewise variation of inlet temperature†

SADIK KAKAÇ‡ and WEIGONG LI§

‡Department of Mechanical Engineering, University of Miami, Coral Gables, FL 33124, U.S.A.
§Department of Mechanical Engineering, Florida International University, Miami, FL 33139, U.S.A.

Abstract—A theoretical and experimental study of turbulent forced convection between two parallel plates, subjected to a sinusoidally varying inlet temperature, is presented. The previous work on laminar flow is extended to a more realistic situation, turbulent flow, since most of the flows in practice are generally in the turbulent regime. A boundary condition which accounts for the effects of both external convection and wall thermal capacitance is considered. The analytical solution is obtained through extending the generalized integral transform technique. An experimental apparatus was designed, built and used for the experimental study to provide validation of the mathematical modeling employed. Analytical solutions are compared with the experimental findings. A satisfactory agreement is obtained when the non-uniform inlet temperature amplitude profile obtained experimentally is incorporated into the theoretical model. Furthermore, the effects of the modified Biot number, the fluid-to-wall thermal capacitance ratio and the Reynolds number on the temperature amplitude along the channel are also discussed for turbulent flow.

INTRODUCTION

UNSTEADY forced convection is an important branch of heat transfer research and technology. Ducts are generally the basic parts of a heat exchanger that may be exposed to many planned or unplanned transients. In thermal equipment, unsteady behavior of temperature distribution in heat exchange equipment can produce such undesirable effects as reduced thermal performance and severe thermal stress with eventual mechanical failure. In practice, most of the flows in the thermal exchange equipment are turbulent. Thus, it is very important to know the unsteady response of turbulent flow in order to avoid reduction in thermal performance and/or mechanical failures.

Sparrow and De Farias [1] analyzed the periodic forced convection with slug flow in a parallel-plate channel with sinusoidally varying inlet temperature and time- and space-dependent wall temperature. The wall temperature was dynamically determined by considering both the heat transfer rate and the energy storage. Kakaç and Yener [2] obtained an exact solution to the transient energy equation for laminar slug flow in parallel plate channel with a sinusoidal variation of fluid inlet temperature. Kakaç [3] obtained a general solution of the energy equation of unsteady forced convection for the decay of a time varying inlet temperature for fully developed turbulent flow between two parallel plates. Cotta and Özisik [4] studied laminar forced convection with periodic variation of inlet temperature analytically, in which they introduced the lowest order solution. Later, the previous work [4] is extended to a more general boundary condition which accounts for the external convection and heat storage of the wall. Good agreement between experimental findings and the analytical solution was obtained [5]. Recently, a theoretical analysis of turbulent forced convection inside parallel-plate channel with periodic variation of inlet temperature under the constant wall temperature boundary condition has been discussed and solved by using the lowest-order solution [6].

In the present paper, the temperature amplitudes for different Reynolds numbers along the centerline of the channel were experimentally measured. A model considering both external convection and wall thermal capacitance was established for unsteady turbulent forced convection subjected to sinusoidally varying inlet temperature. The analytical solutions and the experimental findings were compared to provide validation of the mathematical approach employed. Furthermore, the effects of the modified Biot number (Bi), the fluid-to-wall thermal capacitance ratio (a^*) and Reynolds number (Re) on the temperature amplitude along the channel are also discussed for turbulent flow.

FORMULATION AND METHOD OF SOLUTION

Governing equation and boundary conditions

Let us consider unsteady turbulent forced convection inside a parallel-plate channel, with a hydrodynamically fully developed turbulent flow. The inlet

†Dedicated to Prof. J. P. Hartnett on his 70th birthday.

NOMENCLATURE

a thermal diffusivity of the fluid [$m^2 s^{-1}$]
a^* fluid-to-wall thermal capacitance ratio, $(\rho C_p)_f d/(\rho c)_w L$
a^*_{nk} element of matrix A, equation (12b)
A $N \times N$ matrix, equation (12b)
$A(\xi,\eta)$ dimensionless temperature amplitude, equation (17)
A_{nk} coefficient, equation (11b)
Bi modified Biot number, $h_c d/k$
C, C_p specific heat [$J kg^{-1} K^{-1}$]
c_n coefficient, equation (13)
d half distance between parallel plates, or diameter of thermocouple probe [m]
D_e equivalent diameter of rectangular duct [m]
f_k constant, equation (14)
g_k function, equation (15b)
h heat transfer coefficient outside the wall [$W m^{-2} K^{-1}$]
h_c equivalent heat transfer coefficient, $(1h + L/k_w)^{-1}$ [$W m^{-2} K^{-1}$]
h_{th} heat transfer coefficient around the thermocouple probe [$W m^{-2} K^{-1}$]
i imaginary number, $\sqrt{(-1)}$
Im imaginary part of the complex value
k thermal conductivity [$W m^{-1} K^{-1}$] or integer number
L thickness of the wall [m]
n integer
N number of terms in series
N_n norm of the eigenfunction $Y_n(\eta)$, equation (9c)
Pr Prandtl number, v/a
Re Reynolds number, $U_m D_e/v$, or real part of the complex value
S surface area of thermocouple probe [m^2]
t time [s]
T temperature [°C]
$u(y)$ fully developed velocity profile [$m s^{-1}$]
$U(\eta)$ dimensionless velocity profile, $u(y)/U_m$
U_m mean velocity [$m s^{-1}$]
V volume of thermocouple probe [m^3]
x axial coordinate [m]
X dimensionless axial coordinate, x/D_e
y normal coordinate [m]
$Y_n(\eta)$ eigenfunction corresponding to nth eigenvalue, equation (8).

Greek symbols

β inlet frequency [Hz]
δ_{nk} δ function, for $n = k$, $\delta_{nk} = 1$; for $n \neq k$, $\delta_{nk} = 0$
$\Delta T(y)$ inlet temperature amplitude profile
ΔT_c temperature amplitude at the center of the inlet
$\Delta\theta(\eta)$ dimensionless inlet temperature amplitude profile, $\Delta T(y)/\Delta T_c$
ε_h dimensionless function, $1 + a_t/a$
ε_m turbulent eddy viscosity [$m s^{-2}$]
η dimensionless normal coordinate, y/d
$\theta(\xi,\eta,\tau)$ dimensionless temperature, $(T - T_\infty)/\Delta T_c$
θ_k^+ kth eigenvector of the matrix eigenproblem (12)
λ_n nth eigenvalue of equation (8)
μ_n nth eigenvalue of matrix A
ξ dimensionless axial coordinate, $(x/D_e)(D_e/d)^2/(RePr)$
τ dimensionless time, at/d^2
τ^* time constant of thermocouple, [s^{-1}]
$\phi(\xi,\eta)$ function, equation (5)
$\varphi(\Omega,\xi)$ phase lag, equation (17)
$\Psi_k(\xi)$ function, equation (9b)
Ω dimensionless inlet frequency, $2\pi\beta d^2/a$.

Subscripts

c centerline of the channel
f working fluid (air)
t turbulent flow
th thermocouple material
w wall
∞ value at the ambient.

temperature is subjected to a periodic variation. The geometry for the theoretical analysis is shown in Fig. 1. The conduction along the flow (x-direction) in the wall material is disregarded, and constant fluid thermophysical properties are assumed. The energy equation governing the diffusion in the y-direction and the convection in the x-direction can be written as:

$$\frac{\partial T}{\partial t} + u(y)\frac{\partial T}{\partial x} = \frac{\partial}{\partial y}\left[(a + a_t)\frac{\partial T}{\partial y}\right]$$

for $0 < y < d$, $x > 0$, $t > 0$ (1a)

with inlet and boundary conditions at the center of the channel, as:

$$T(0,y,t) = T_\infty + \Delta T(y)e^{i2\pi\beta t},$$

for $0 < y < d$, $t > 0$, (1b)

$$\frac{\partial T}{\partial y} = 0, \quad \text{at} \quad y = 0, \quad \text{for} \quad x > 0, \quad t > 0. \quad (1c)$$

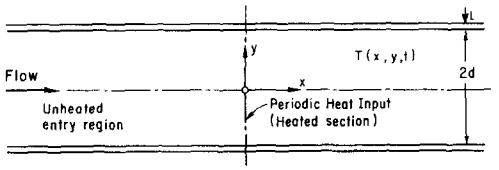

FIG. 1. Geometry of the duct for theoretical analysis.

With the assumption of uniform wall temperature across the whole thickness of the wall material, the boundary condition considering both external convection and wall heat storage may be expressed as:

$$h_e(T-T_\infty)+k\frac{\partial T}{\partial y}+(\rho C)_w L\frac{\partial T}{\partial t}=0,$$

$$\text{at} \quad y=d, \quad \text{for} \quad x>0, \quad t>0. \quad (1d)$$

Introducing the following dimensionless parameters, as:

$$\eta=\frac{y}{d}, \quad \xi=\frac{(x/D_e)(D_e/d)^2}{RePr}, \quad \tau=\frac{at}{d^2},$$

$$Bi=\frac{h_e d}{k}, \quad \Omega=\frac{2\pi\beta d^2}{a}, \quad a^*=\frac{(\rho C_p)_f d}{(\rho C)_w L}, \quad (2a)$$

$$\Delta\theta(\eta)=\frac{\Delta T(y)}{\Delta T_c}, \quad U(\eta)=\frac{u(y)}{U_m},$$

$$\theta(\xi,\eta,\tau)=\frac{T(x,y,t)-T_\infty}{\Delta T_c}, \quad (2b)$$

the governing equation, inlet and boundary conditions can be rewritten in dimensionless form as:

$$\frac{\partial\theta}{\partial\tau}+U(\eta)\frac{\partial\theta}{\partial\xi}=\frac{\partial}{\partial\eta}\left[\varepsilon_h(\eta)\frac{\partial\theta}{\partial\eta}\right],$$

$$\text{for} \quad 0<\eta<1, \quad \xi>0, \quad \tau>0 \quad (3a)$$

$$\theta(0,\eta,\tau)=\Delta\theta(\eta)e^{i\Omega\tau}, \quad \text{for} \quad 0<\eta<1, \quad \tau>0 \quad (3b)$$

$$\frac{\partial\theta}{\partial\eta}=0, \quad \text{at} \quad \eta=0, \quad \text{for} \quad \xi>0, \quad \tau>0, \quad (3c)$$

where

$$Bi\theta+\frac{\partial\theta}{\partial\eta}+\frac{1}{a^*}\frac{\partial\theta}{\partial\tau}=0, \quad \text{at} \quad \eta=1,$$

$$\text{for} \quad \xi>0, \quad \tau>0 \quad (3d)$$

$$\varepsilon_h(\eta)=1+\frac{a_t}{a}=1+\frac{Pr}{Pr_t}\frac{\varepsilon_m}{\nu} \quad (4)$$

in which ε_m is turbulent eddy viscosity, as predicted by a turbulence model. The fully developed turbulent velocity distribution $U(\eta)$ given in ref. [7] and the turbulent eddy viscosity ε_m given in ref. [8] are used in the present analysis (see the Appendix).

Note that if the wall heat capacitance is negligible compared to the fluid thermal capacitance, a^* becomes a very large number, and the conductance in h_e diminishes. Consequently, the contribution of $(1/a^*)(\partial\theta/\partial\tau)$ becomes very small in equation (3), and the boundary condition (3d) reduces to the regular third kind of convective boundary condition.

A periodic solution of the form

$$\theta(\xi,\eta,\tau)=e^{i\Omega\tau}\phi(\xi,\eta) \quad (5)$$

is assumed for the decay of the inlet condition along the channel. The initial condition is not needed since only the 'steady' portion of the temperature response, $\phi(\xi,\eta)$, is of interest. Then, equations (3) can be simplified as:

$$\frac{\partial}{\partial\eta}\left(\varepsilon_h(\eta)\frac{\partial\phi}{\partial\eta}\right)-U(\eta)\frac{\partial\phi}{\partial\xi}-i\Omega\phi=0,$$

$$\text{for} \quad 0<\eta<1, \quad \xi>0, \quad \tau>0 \quad (6a)$$

$$\phi(0,\eta)=\Delta\theta(\eta), \quad \text{at} \quad \xi=0, \quad \text{for} \quad 0<\eta<1 \quad (6b)$$

$$\frac{\partial\phi}{\partial\eta}=0, \quad \text{at} \quad \eta=0 \quad (6c)$$

$$Bi\phi+\frac{\partial\phi}{\partial\eta}=-\frac{i\Omega}{a^*}\phi, \quad \text{at} \quad \eta=1, \quad (6d)$$

where a dimensionless inlet temperature amplitude, $\Delta\theta(\eta)$ determined experimentally as:

$$\Delta\theta(\eta)=1.035+0.098\eta-1.04\eta^2 \quad (7)$$

is coupled in the theoretical analysis.

Methods of solution

A formal solution to the above problem by using the classical integral transform technique leads to a complex non-classical Sturm–Liouville problem for which no direct known solution is available. Based on the generalized integral transform technique [4, 5], the same method will be extended for solving turbulent forced convection for timewise variation of inlet temperature. Let us consider the following eigenvalue problem:

$$\frac{d}{d\eta}\left(\varepsilon_h(\eta)\frac{dY_n(\eta)}{d\eta}\right)+\lambda_n^2U(\eta)Y_n(\eta)=0,$$

$$\text{for} \quad 0<\eta<1 \quad (8a)$$

$$\frac{dY_n}{d\eta}=0, \quad \text{at} \quad \eta=0 \quad (8b)$$

$$Bi\,Y_n+\frac{dY_n}{d\eta}=0, \quad \text{at} \quad \eta=1, \quad (8c)$$

where $Y_n(\eta)$ is the eigenfunction corresponding to the nth eigenvalue λ_n. Equations (8) allow the definition of an integral-transform pair for the function $\phi(\xi,\eta)$ given by:

$$\phi(\xi,\eta)=\sum_{n=1}^{\infty}\frac{1}{\sqrt{N_n}}\Psi_n(\xi)Y_n(\eta) \quad (9a)$$

in which the normalization integral is defined as:

$$\Psi_n(\xi)=\int_0^1\frac{1}{\sqrt{N_n}}U(\eta)\phi(\xi,\eta)Y_n(\eta)d\eta \quad (9b)$$

$$N_n=\int_0^1U(\eta)Y_n^2(\eta)d\eta. \quad (9c)$$

Multiplying equation (8a) with $[Y_n(\eta)/\sqrt{N_n}]$, then integrating with respect to η from 0 to 1, one can obtain

$$\frac{d\Psi_n}{d\xi}+\lambda_n^2\Psi_n=\frac{\varepsilon_h(1)}{\sqrt{N_n}}\left(Y_n(1)\frac{\partial\phi(\xi,1)}{\partial\eta}-\phi(\xi,1)\frac{dY_n(1)}{d\eta}\right)-i\Omega\int_0^1\frac{Y_n}{\sqrt{N_n}}\phi(\xi,\eta)d\eta. \quad (10)$$

By using equations (6d) and (8c), the following relationship can be established:

$$\frac{\varepsilon_h(1)}{\sqrt{N_n}}\left(Y_n(1)\frac{\partial\phi(\xi,1)}{\partial\eta}-\phi(\xi,1)\frac{dY_n(1)}{d\eta}\right)=-\frac{i\Omega}{a^*}\frac{Y_n(1)}{\sqrt{N_n}}\varepsilon_h(1)\phi(\xi,1).$$

Using the expression of $\phi(\xi,\eta)$, equation (9a), it has

$$\frac{\varepsilon(1)}{\sqrt{N_n}}\left(Y_n(1)\frac{\partial\phi(\xi,1)}{\partial\eta}-\phi(\xi,1)\frac{dY_n(1)}{d\eta}\right)=-\frac{i\Omega}{a^*}\sum_{k=1}^{\infty}\frac{\varepsilon_h(1)}{\sqrt{N_nN_k}}Y_n(1)Y_k(1)\Psi_k(\xi).$$

Substituting the above relation into equation (10), the differential equation for $\Psi_n(\xi)$ can be written as:

$$\frac{d\Psi_n}{d\xi}+\sum_{k=1}^{\infty}(\delta_{nk}\lambda_n^2+i\Omega A_{nk})\Psi_k=0, \quad (11a)$$

where

$$A_{nk}=A_{kn}=\frac{1}{\sqrt{N_nN_k}}\left(\frac{\varepsilon_h(1)Y_n(1)Y_k(1)}{a^*}+\int_0^1 Y_n(\eta)Y_k(\eta)d\eta\right). \quad (11b)$$

After performing the same operation for the inlet condition, the following equation can be obtained:

$$\Psi_n(0)=\frac{1}{\sqrt{N_n}}\int_0^1 U(\eta)\Delta\theta(\eta)Y_n(\eta)d\eta=f_n. \quad (11c)$$

Equations (11) form a set of infinite, coupled, first-order linear ordinary differential equations. As discussed in ref. [9], it can be truncated to any sufficiently large order, N, and solved to any desired accuracy.

Let μ_k and $\{\theta_1^+,\theta_2^+,\ldots,\theta_N^+\}$ express the eigenvalues and eigenvectors for the $N\times N$ coefficient matrix A, which are determined by the following linear algebra equations,

$$(A-\mu_k I)\theta_k^+=0 \quad (12a)$$

where I is an $N\times N$ unit matrix, and

$$A=(a_{nk}^*), \quad \text{and} \quad a_{nk}^*=\delta_{nk}\lambda_n^2+i\Omega A_{nk}. \quad (12b)$$

By knowing the eigenvalues and corresponding eigenvectors of matrix A, the general solution of equations (11) may be constructed from the linear combination of N independent solutions, as:

$$\Psi_n(\xi)=\sum_{k=1}^{N}c_k\theta_{nk}^+e^{-\mu_k\xi}, \quad (n=1,2,\ldots,N), \quad (13)$$

where θ_{nk}^+ is the kth component of the nth eigenvector, and the constants c_n could be determined by constraining this solution to satisfy the inlet condition, as:

$$\sum_{k=1}^{N}c_k\theta_{nk}^+=f_k. \quad (14)$$

It should be noted that for small values of a^* the diagonal elements in the matrix A could be the same order as λ_n^2, i.e. the diagonal elements are no longer dominant in the matrix eigenvalue problem. In this case, the lowest order solution suggested in ref. [6] may not be valid. Then the solution for $\phi(\xi,\eta)$ can be expressed by the inversion formula, equation (9a), as:

$$\phi(\xi,\eta)=\sum_{k=1}^{N}\frac{Y_k}{\sqrt{N_n}}\left[\sum_{n=1}^{N}c_k\theta_{nk}^+e^{-\mu_k\xi}\right]=\sum_{k=1}^{N}g_k(\eta)e^{-\mu_k\xi} \quad (15a)$$

$$g_k(\eta)=c_k\sum_{n=1}^{N}\frac{1}{\sqrt{N_n}}\theta_{nk}^+Y_n(\eta). \quad (15b)$$

Finally, the expression of the dimensionless temperature may be written as:

$$\theta(\xi,\eta,\tau)=e^{i\Omega\tau}\sum_{k=1}^{N}g_k(\eta)e^{-\mu_k\xi}. \quad (16)$$

Note that the eigenvalues μ_k and the functions $g_k(\eta)$ $(k=1,2,\ldots,N)$ are complex; therefore, the solution of $\theta(\xi,\eta,\tau)$ is also complex. The final solution will only be the real (or imaginary) part of the above solution, given as,

$$\theta(\xi,\eta,\tau)=Re[\phi(\xi,\eta)e^{i\Omega\tau}]=Re[A(\xi,\eta)e^{i[\Omega\tau+\varphi(\Omega,\xi)]}]=A(\xi,\eta)\cos[\Omega\tau+\varphi(\Omega,\xi)] \quad (17)$$

where the dimensionless temperature amplitude, $A(\xi,\eta)$, and the phase lag of the dimensionless temperature, $\varphi(\Omega,\xi)$, may be defined as:

$$A(\xi,\eta)=\sqrt{[Re(\phi)]^2+[Im(\phi)]^2}, \quad \text{for} \quad \xi>0, \quad 0<\eta<1 \quad (18a)$$

$$\varphi(\Omega,\xi)=\tan^{-1}\frac{Im(\phi)}{Re(\phi)}. \quad (18b)$$

A computer program using the general integral technique is constructed, and the analytical results are compared to the experimental findings.

EXPERIMENTS

Experimental set-up

An experimental set-up has been designed, built and used to study the behavior of unsteady laminar and turbulent forced convection between the parallel-plate channel with sinusoidally varying inlet temperature. A schematic diagram of the apparatus with the basic components and instrumentation is shown in Fig. 2.

To simulate the parallel-plate channel, a rec-

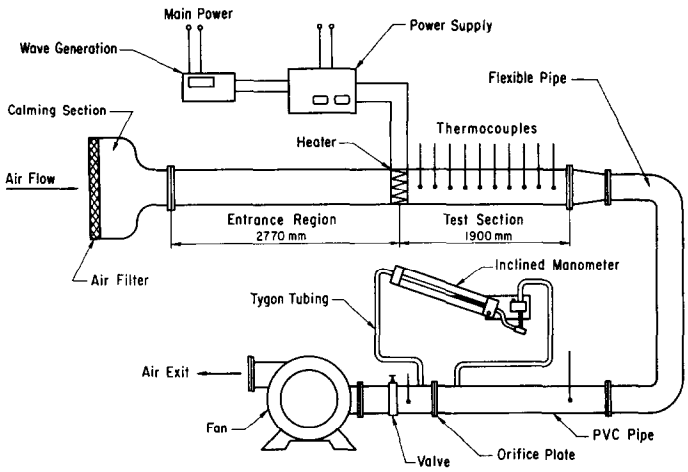

FIG. 2. Schematic diagram of experimental set-up.

tangular duct with the aspect ratio 10 (254.0×25.4 mm^2, or 10×1 in.^{2}) is constructed. For validation of the theoretical analysis used, in the experiments, only the fluid temperature variation along the centerline of the channel is investigated. The experimental findings obtained are used to compare with the theoretical analyses for the parallel-plate-channel. With the available components, it is possible to work with inlet frequencies from 0.01 to 0.20 Hz. The Reynolds number based on the hydraulic diameter of the channel is varied from 400 to 2000 in laminar flow and from 4000 to 20 000 in turbulent flow regimes.

The main component of the apparatus is the rectangular channel with different sections for filtering, calming, entrance, testing, and convergence. The experimental apparatus is operated in the suction mode in order to provide smooth air flow. The instrumentation includes a wave generator, a power supply, a heater, an inclined manometer, voltmeters, thermocouples, an orifice plate and a fan.

Air flows from the calming section to the inlet section (2770 mm in length) where the velocity becomes fully developed. The duct is constructed with an outer casing made from 6.35 mm (1/4 in.) thick plywood with outer dimensions of $114.3 \text{ mm} \times 381 \text{ mm} \times 4670$ mm and incorporate the inlet and test sections. The inner surface of the casing is lined with 25.4 mm thick extruded styrofoam, leaving a cross-sectional flow area of 254×25.4 mm^2 (10×1 in.^{2}). To ensure a hydraulically smooth surface, the styroform surface has been painted carefully.

Throughout the study, periodic variation of heat input is provided by an electric heater constructed to fit into the channel. In order to minimize the disturbance to the air flow, a 0.4 mm diameter nichrome resistance wire is used as the heating element. The sine variation of heat input to the heater at various frequencies is provided by a function generator and the power supply. To measure the temperature variation along the channel, 14 thermocouples are placed at equal intervals along the test section starting at the exit of the electric heater. The thermocouples are made from 0.01 in. (0.254 mm) diameter, 30 gage, Teflon-coated chromel and constantan (E-type) thermocouple wires, and calibrated in the Heat Transfer Laboratory.

Experimental uncertainty

Steady temperature measurement. The measurements made with the E-type thermocouple usually have an uncertainty of ± 0.1°C within the range of 0 to 100°C after careful calibration.

Unsteady temperature measurement. As discussed in ref. [10], it is known that when the fluid temperature varies with time, the response of the thermocouple depends upon the physical properties of the thermocouple material and the dynamic properties of the surrounding environment. For the ideal sphere thermocouple probe, the unsteady temperature, T, has the following relation with the reading temperature (or measuring temperature), T_{read}:

$$T = [1 + (2\pi\beta\tau^*)^2]T_{\text{read}} \tag{19}$$

in which

$$\tau^* = \frac{(\rho VC)_{\text{th}}}{(hS)_{\text{th}}} = \frac{(\rho dC)_{\text{th}}}{6h_{\text{th}}}, \tag{20}$$

where ρ_{th} and C_{th} are the density and specific heat of the thermocouple material, respectively; h_{th} is the heat transfer coefficient around the thermocouple probe; V_{th}, S_{th} and d_{th} are the volume, surface area and the diameter of the thermocouple probe, respectively; T is the real fluid temperature, and T_{read} is the reading temperature of the fluid.

It implies that the fluid temperature measurement in our experiments depends upon the frequency of the periodic variation (β) and the time constant of the thermocouple (τ^*). For an E-type thermocouple constructed with 0.01 in. diameter chromel and constantan wires and 0.03 in. diameter sphere probe, the time constant τ^* is less than 3×10^{-3} s in our experiments. Therefore, the difference between real tem-

perature (T) and reading temperature (T_{read}) could be safely neglected. For the high frequency, the dynamic effect of the thermocouple probe may not be negligible, and the fluid temperature should be corrected according to equation (19).

Mass flow rate calculation. The uncertainty associated with the mass flow rate is calculated as $\pm 2.64\%$ according to ASME Standard [11].

Experimental procedure

For each data run, both temperature oscillation frequency (β) at inlet and the Reynolds number (Re) are fixed, but they are adjustable in the entire experiment. First, the pressure drop across the orifice plate can be adjusted to the desired range, and the inlet frequency can be stabilized on the selected value. After turning on the electric heater, temperature amplitudes at various locations should be checked until they are not changing with time. Then, at a fixed value of Reynolds number and a given inlet frequency, the oscillation of temperature along the channel as a function of time and the temperatures before and after the orifice plate can be recorded by thermocouples.

After the completion of data recordings, the inlet frequency is reset to the next desired value. All temperatures and pressure drop will be remeasured until the steady temperature amplitude is reached. After all desired inlet frequencies are carried out, the experiments for another desired pressure drop across the orifice plate (Reynolds number) will be repeated.

RESULTS AND DISCUSSIONS

Temperature response

During the experiments, the temperature at the entrance is specified as a sinusoidal oscillation, as shown in the recordings, Fig. 3. The amplitude of temperature oscillations along the centerline of the channel is obtained from the maximum and minimum values of the oscillating temperature converted from the maximum and minimum of the oscillating thermocouple readings by a high accuracy voltmeter (T_{max} and T_{min}). The temperature amplitude ΔT is defined as

$$\Delta T = (T_{max} - T_{min})/2. \tag{21}$$

The variation of the temperature amplitude along the centerline of the channel is recorded at different locations for a given Reynolds number. Figure 3 shows the typical thermocouple temperature response for the oscillating inlet temperature in the thermal entrance region. It can be seen that the temperature responses downstream along the channel at different locations are also sinusoidal variations and they have the same frequency as that at the inlet.

Inlet temperature amplitude profile

Since the inlet temperature amplitude is a very important factor that affects the theoretical analysis, we measured the inlet temperature amplitude profile experimentally and rechecked the construction of the electric heater. From the measurements, it is known that the inlet temperature amplitude is not uniform across the channel.

In Fig. 4, the experimentally measured dimensionless inlet temperature amplitude for turbulent flow is plotted. The equation (7) presented on the plot as a description of the inlet temperature amplitude profile is obtained by using a least square method to fit the experimental results. In order to compare the experimental findings with the analytical results, the experimental inlet temperature amplitude profile is employed in the theoretical analyses.

Dimensionless temperature amplitudes

The dimensionless temperature amplitudes along the centerline of the channel are calculated for the parameters $Bi = 10$, $a^* = 8.5 \times 10^{-3}$ and $\beta = 0.04$ and 0.08 Hz, which are specified by experimental conditions. Some theoretical dimensionless temperature amplitudes and the corresponding experimental results along the centerline of the channel for turbulent flow ($Re \approx 8900$–$20\,000$) are plotted in Figs. 5 and 6. The theoretical solutions for the assumed constant inlet temperature profile and the measured parabolic inlet temperature profile are presented. As seen in Figs. 5 and 6, the experimental data and theoretical analysis are in acceptable agreements. In the experiments, especially in turbulent regime, the temperature amplitude usually drops below 3°C [10]. With the accuracy of 0.1°C in temperature measurement for the E-type thermocouples, the relative error of temperature measurement will be $0.1/3 \approx 3.3\%$. As x/D_e further increases, the temperature amplitude continuously decreases, so the relative error of temperature measurement will increase. Besides the experimental approximations, theoretical assumptions and the accuracy of the simple turbulent model may be the major cause of the small consistent deviation between the experimental and numerical analyses. In another way, the scale of the vertical coordinate on the plots is logarithmic, which makes the deviation look bigger than its real value. The maximum deviation, in our experimental range, between the experimental findings and analytical dimensionless temperature amplitudes with the experimental inlet temperature amplitude is usually less than 0.10. This is quite satisfactory for the simple turbulent model used in the theoretical study. It is also shown that the effect of a non-uniform inlet temperature profile is quite significant in bringing the theoretical and experimental results to an acceptable agreement.

It is seen from Figs. 5 and 6 that the Reynolds number (Re) is one major factor which affects the variation of the temperature amplitude. Generally, the temperature amplitude decays exponentially along the distance from the inlet except at the locations very close to the inlet. For a given inlet frequency (β), the temperature amplitude depends strongly upon the Reynolds number (Re). If the Reynolds number

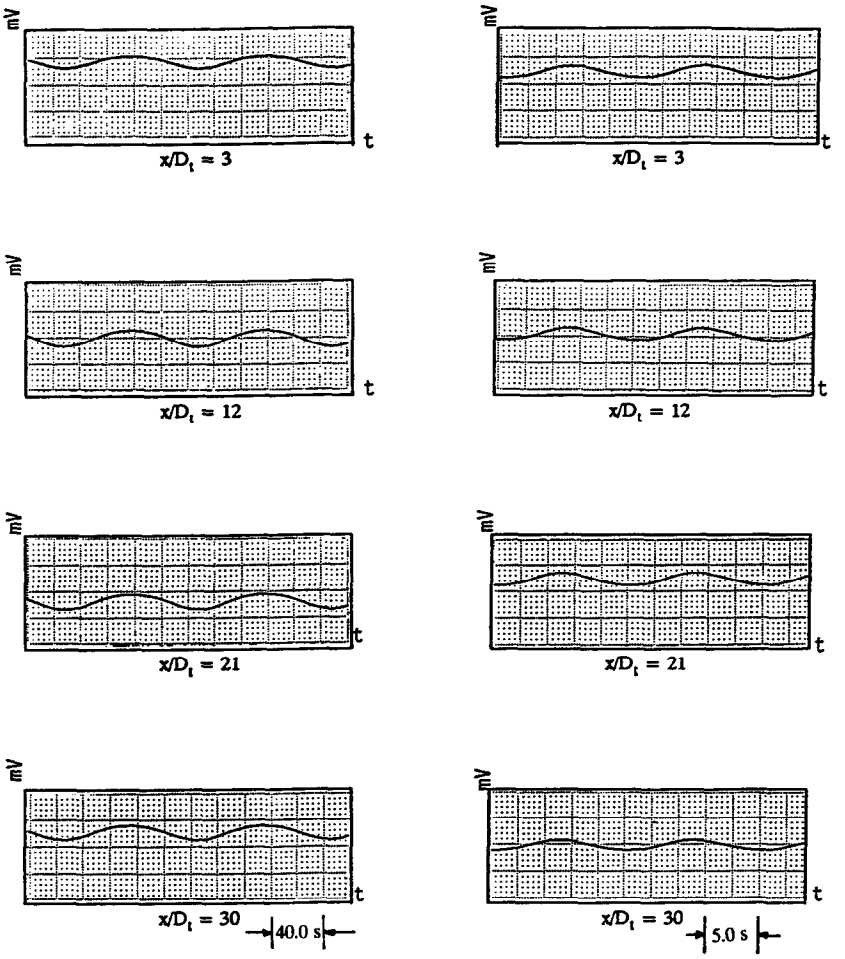

FIG. 3. Experimental results of temperature response at different locations along the centerline of the duct.

increases, the decay of the temperature amplitude will decrease. For higher Reynolds numbers (Re), the rate in decrease of temperature amplitude along the channel (the slope of the amplitude curve vs x/D_e) will be reduced.

From the temperature amplitude comparison in turbulent flow, it may be concluded that the model of turbulence and the method of calculation are acceptable to predict the temperature distribution inside the channel and the decay of the temperature amplitude along the duct for a timewise varying inlet temperature in the turbulent thermal entrance region.

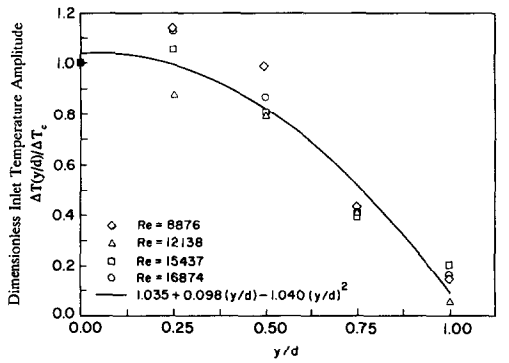

FIG. 4. Experimental dimensionless inlet temperature amplitude profile for turbulent flow.

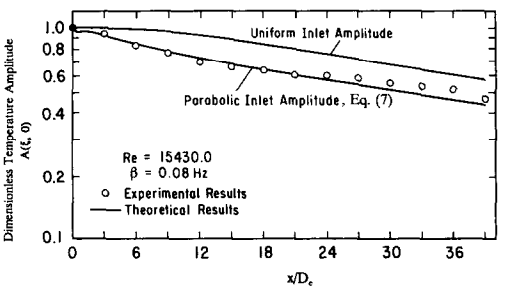

FIG. 5. Variation of the amplitude of the dimesionless temperature along the centerline of the duct for Re = 15430, Pr = 0.7 and β = 0.08 Hz.

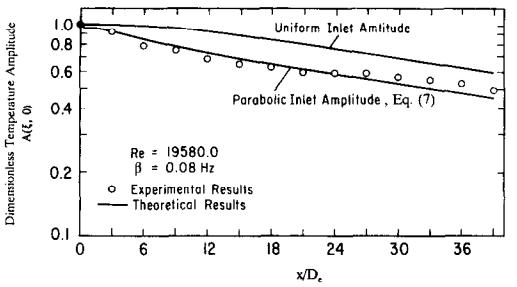

FIG. 6. Variation of the amplitude of the dimensionless temperature along the centerline of the duct for $Re = 19\,570$, $Pr = 0.7$ and $\beta = 0.08$ Hz.

In Fig. 7, the results of phase lags of the centerline temperature along the channel, $-\varphi(\Omega,\xi)$, are presented for different values of inlet frequencies (Ω) at Reynolds number $Re = 20\,000$ and $a^* = 8.5 \times 10^{-3}$. One can see that the phase lag increases with increase in the dimensionless inlet frequency. Because of the difficulty in measuring the phase lag experimentally, only the numerical values of phase lag are reported.

Further discussion of the effect of Bi, a and Re on the temperature amplitudes*

For turbulent flow, the modified Biot number (Bi) and thermal capacitance ratio (a^*) will affect the temperature amplitude, and have more complicated influence than that for laminar flow [9]. In addition to the parameters of Bi and a^*, the Reynolds number (Re) will also affect the temperature amplitude variation even when the amplitude is plotted against the so-called dimensionless axial coordinates $\xi = (x/D_e)(D_e/d)^2/(RePr)$. For turbulent flow the dimensionless temperature amplitude variation is no longer a straight line in the semilog plots, since the eddy viscosity (ε_m) and eddy diffusivity (ε_h), which dominate the heat and momentum transport, are the functions of the Reynolds number. Thus, the basic dimensionless governing equation depends on the Reynolds number (Re), while it is identical for laminar flow.

In Fig. 8, the effects of modified Biot number on the temperature amplitude along the centerline of the channel are plotted vs the dimensionless axial distance, $\xi = (x/D_e)(D_e/d)^2/(RePr)$. Figure 8 gives the variation of the temperature amplitude for different

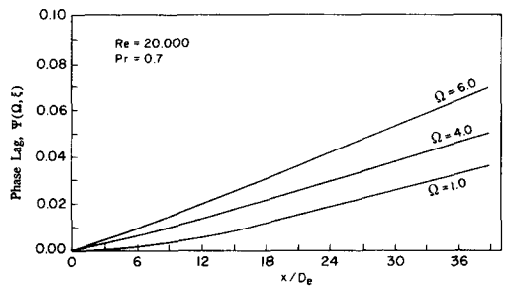

FIG. 7. The phase lags of the dimensionless temperature along the centerline of the duct for different values of dimensionless inlet frequency.

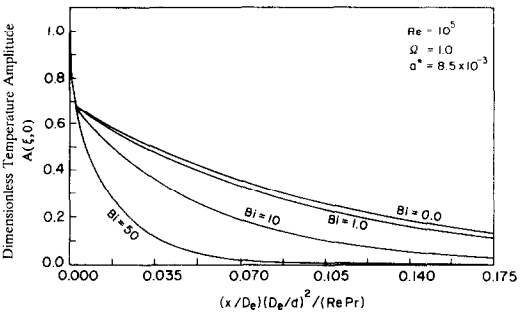

FIG. 8. The effect of modified Biot number (Bi) on dimensionless temperature amplitude along the centerline of the channel for $Re = 10^5$, $a^* = 8.5 \times 10^{-3}$ and $\Omega = 1.0$ in turbulent flow.

Bi (= 0, 1, 10 and 50) with $\Omega = 1.0$ and $Re = 10^6$ and $a^* = 8.5 \times 10^{-3}$. It is seen that for the fixed value of a^* ($= 8.5 \times 10^{-3}$), the effect of Bi number on dimensionless temperature amplitude variation is not negligible. The dimensionless temperature amplitudes are very sensitive to the external convection, because in turbulent flow much more heat is transferred across the channel and could be stored inside the walls. Generally, in turbulent flow the effect of Bi is more complicated than that in laminar flow because of the dependance on the Reynolds number, therefore, it is almost impossible to give the limit of a^*, which can separate whether the effect of Bi could be neglected or not, as for laminar flow [9].

Figures 9 and 10 illustrate the effects of fluid-to-

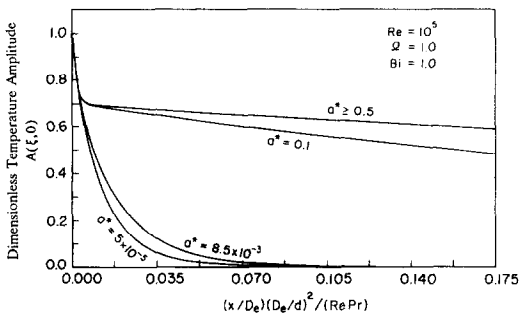

FIG. 9. The effect of fluid-to-wall thermal capacitance ratio (a^*) on dimensionless temperature amplitude along the centerline of the channel for $Re = 10^5$, $Bi = 1.0$ and $\Omega = 1.0$ in turbulent flow.

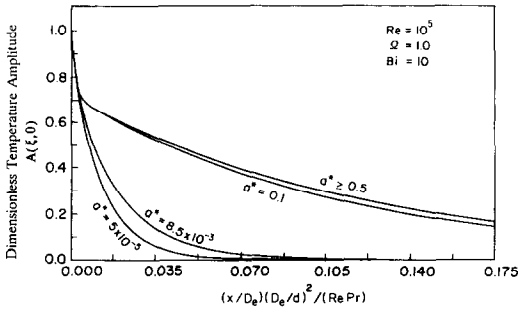

FIG. 10. The effect of fluid-to-wall thermal capacitance ratio (a^*) on dimensionless temperature amplitude along the centerline of the channel for $Re = 10^5$, $Bi = 10.0$ and $\Omega = 1.0$ in turbulent flow.

wall thermal capacitance ratio (a^*) on the temperature amplitudes along the centerline of the channel for $Bi = 1.0$ and $Bi = 10$ with $\Omega = 1.0$ and $Re = 10^5$. It is known that for large wall thermal capacitances (small values of a^*), the storage of the heat inside the wall is dominant compared to the heat transferred to the outside by external convection, therefore, the temperature amplitude decays quickly. For the small values of modified Biot number (Bi), the temperature amplitude is more sensitive to the thermal capacitance ratio (a^*); the differences between the temperature amplitude for different a^* are larger than the cases for large values of Bi. For the large value of Bi ($Bi = 10$), the heat carried by the external convection and the heat stored inside the wall are of the same order, the influence of a^* is not as strong as that for the small values of Bi. Combining the good external convection (large value of Bi) and the thermal storage of the wall (small value of a^*), the temperature amplitude decays more rapidly than it does for the small value of Bi, see Fig. 9.

As mentioned above, for different Reynolds numbers (Re), the curve of the temperature amplitude variation vs the so-called dimensionless axial coordinate $\xi = (x/D_e)(D_e/d)^2/(RePr)$, will not be identical. Figure 11 shows the variation of temperature amplitude for different values of Re at the same external convective condition ($Bi = 10$) and the thermal capacitance ratio a^* ($= 8.5 \times 10^{-3}$). According to the study, the effect of the Reynolds number (Re) on the temperature amplitudes for the large values of a^* (>0.1) is very similar to Fig. 10. It can be seen that the temperature amplitude along the channel for the high Reynolds number is less than the amplitude for the lower Reynolds number. For the higher Reynolds number, the heat transferred from the flowing fluid to the wall and then carried by external convection is larger than that for the lower Reynolds number; therefore, in turbulent flow the temperature amplitude for higher Reynolds number is lower than that for lower Reynolds number. However, it is shown that the influence of the Reynolds number on the amplitude for larger values of Bi is more significant than that for smaller values of Bi.

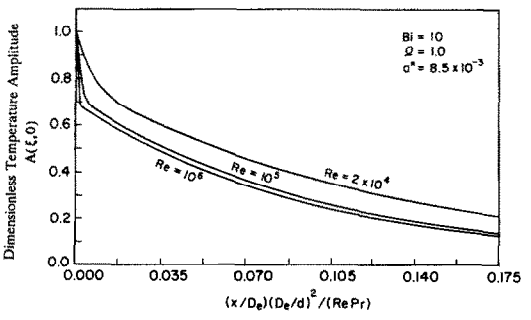

FIG. 11. The effect of Reynolds number (Re) on dimensionless temperature amplitude along the centerline of the channel for $a^* = 8.5 \times 10^{-3}$, Bi = 10.0 and $\Omega = 1.0$ in turbulent flow.

It may be concluded that the heat transport in turbulent flow is much stronger than that in laminar flow, thus more heat is transferred from the flowing fluid to the wall. Obviously, the heat balance between the wall and external ambient strongly depends on external convection (Bi). For the small values of Bi and a^*, the heat stored inside the wall is dominant and the influence of the a^* is more effective. For the large value of Bi and small value of a^*, the heat carried by external convection and stored inside the wall are of the same order, the effect of the a^* is not so strong as that for the small value of Bi, but the effect is still observable. Generally, for the higher Reynolds number, the eddy diffusivity (ε_h) has a larger value, therefore, the effects of Bi and a^* for higher Reynolds number are more evident.

CONCLUDING REMARKS

The temperature responses and decays of the sinusoidal variation of the inlet temperature along a parallel plate-channel are investigated experimentally and theoretically for various values of Reynolds number (Re), modified Biot number (Bi) and fluid-to-wall thermal capacitance ratio (a^*). From the above experimental and theoretical investigations and analysis, the following conclusions are deduced for unsteady turbulent forced convection in the thermal entrance region for periodically varying inlet temperature.

(1) The periodic nature of the temperature oscillations along the channel has the same frequency as at the inlet. Generally, the unsteady temperature distribution depends on inlet frequency (β), the Reynolds number (Re), the fluid-to-wall thermal capacitance ratio (a^*) and the modified Biot number (Bi).

(2) The present model and calculation procedure are acceptable to predict the temperature distribution inside the channel and the decay of the temperature along the channel for timewise varying inlet temperature in turbulent thermal entrance region. The experimental results and theoretical analyses are in acceptable agreement.

(3) For a given value of inlet frequency (β), the value of the temperature amplitude at a point downstream depends on the Reynolds number (Re). As the Reynolds number increases, the temperature amplitude decay decreases. The higher the Reynolds number (Re), the slower the decay in the temperature amplitude along the channel.

(4) For turbulent flow, the influence of the modified Biot number is much stronger than that for laminar flow, since the thermal resistance inside the duct has been reduced compared to the cases of laminar flow.

(5) For turbulent flow, when $a^* < 8.5 \times 10^{-3}$, the heat stored inside the wall is dominant and the influence of the a^* is more effective for small values of $Bi (Bi < 10)$; while for the large values of $Bi (Bi > 10)$, the heat carried by external convection and stored inside the wall are of the same order, the effect of the

a^* is not so strong as that for the small value of Bi, but the difference for different a^* is still observable.

(6) For turbulent flow, it is very difficult to give the similar applicable tables as in laminar flow, because of the involvement of the dependance on the Reynolds numbers (Re), the effects of the modified Biot numbers (Bi), and the fluid-to-wall thermal capacitance ratios (a^*) on the variation of temperature amplitude, which become more complicated than that in laminar flow.

Acknowledgements—The authors gratefully acknowledge the partial financial support of the National Science Foundation and the NATO Scientific Affairs Division.

REFERENCES

1. E. M. Sparrow and F. N. De Farias, Unsteady heat transfer in ducts with time varying inlet temperature and participating walls, *Int. J. Heat Mass Transfer* **11,** 837 (1968).
2. S. Kakaç and Y. Yener, Exact solution of transient forced convection energy equation for timewise variation of inlet temperature, *Int. J. Heat Mass Transfer* **16,** 2205 (1973).
3. S. Kakaç, A general analytical solution to the equation of transient forced convection with fully developed flow, *Int. J. Heat Mass Transfer* **18,** 1449 (1975).
4. R. M. Cotta and M. N. Özisik, Laminar forced convection inside ducts with periodic variation of inlet temperature, *Int. J. Heat Mass Transfer* **29,** 1495 (1986).
5. S. Kakaç, W. Li and R. M. Cotta, Unsteady laminar forced convection in ducts with periodic variation of inlet temperature, *Trans. ASME J. Heat Transfer* **112,** 913–920 (1990).
6. W. S. Kim and M. N. Özisik, Turbulent forced convection inside a parallel-plate channel with periodic variation of inlet temperature, *Trans. ASME J. Heat Transfer* **111,** 883 (1989).
7. D. B. Spalding, A single formula for the 'Law of the Wall', *J. Appl. Mech.* **28,** 455 (1961).
8. R. I. Larson and S. Yerazunis, Mass transfer in turbulent flow, *Int. J. Heat Mass Transfer* **16,** 121 (1973).
9. W. Li and S. Kakaç, Unsteady thermal entrance heat transfer in laminar flow with a periodic variation of inlet temperature, *Int J. Heat Mass Transfer* **34,** 2581–2592 (1991).
10. W. Li, Experimental and theoretical investigation of unsteady forced convection in ducts, Ph. D. Dissertation, University of Miami, Coral Gables, Florida (1990).
11. ASME Standard, MCF-3M, Measurement of fluid flow in pipe using orifice, nozzle and venturi (1984).

APPENDIX

We may empirically express the fully developed turbulent velocity profile by a three-layer model according to Spalding [7], as,

$$r^+ = u^+ A\left[e^{Bu^+} - 1 - Bu^+ - \frac{1}{2}(Bu^+)^2 - \frac{1}{6}(Bu^+)^3 - \frac{1}{24}(Bu^+)^4\right], \quad \text{(A1)}$$

where

$$u^+ = u/u_\tau, \quad r^+ = ru_\tau/v, \quad r = 1-y, \quad \text{and} \quad u_\tau = \sqrt{\tau_w/\rho}, \quad \text{(A2)}$$

r is the coordinate from the wall towards the centerline of the duct and u_τ is the shear velocity.

For turbulent convective heat transfer, it is essential to know the eddy viscosity, ε_m, and eddy diffusivity, a_t. A two-layer model of eddy viscosity is used. The empirical expression of eddy viscosity is as follows according to Spalding [7]:

$$\frac{\varepsilon_m}{v} = AB\left[e^{Bu^+} - 1 - Bu^+ - \frac{1}{2}(Bu^+)^2 - \frac{1}{6}(Bu^+)^3\right], \quad \text{(A3)}$$

where A and B are constants which are equal to 0.1108 and 0.4, respectively.

The turbulent Prandtl number Pr_t is defined as the ratio of eddy viscosity and eddy diffusivity, as

$$Pr_t = \frac{\text{eddy viscosity } (\varepsilon_m)}{\text{eddy diffusivity } (a_t)}. \quad \text{(A4)}$$

According to the experiments performed by Larson and Yerazunis [8], Pr_t is assumed to be a constant, and is taken as $Pr_t = 0.86$ for the fluid with $Pr = 0.7$.